(4)

CHEMICAL RESEARCH, DEVELOPMENT & ENGINEERING CENTER

CRDEC-CR-88039

INFRARED DIFFERENTIAL ABSORPTION LIDAR FOR VAPOR DETECTION

by J. P. Carrico
K. R. Phelps

DETECTION DIRECTORATE

J. van der Laan
E. E. Uthe
P. L. Holland
J. G. Hawley
L. D. Fletcher
R. E. Warren
N. Nielsen
A. Rosengreen
E. R. Murray

SRI INTERNATIONAL
Menlo Park, CA 94025

February 1988

U.S. ARMY ARMAMENT MUNITIONS CHEMICAL COMMAND

Aberdeen Proving Ground, Maryland 21010-5423

Disclaimer

The findings in this report are not to be construed as an official Department of the Army position unless so designated by other authorizing documents.

Distribution Statement

Approved for public release; distribution is unlimited.

UNCLASSIFIED
SECURITY CLASSIFICATION OF THIS PAGE

REPORT DOCUMENTATION PAGE

1a. REPORT SECURITY CLASSIFICATION UNCLASSIFIED	1b. RESTRICTIVE MARKINGS AD-A190 600
2a. SECURITY CLASSIFICATION AUTHORITY	3 DISTRIBUTION / AVAILABILITY OF REPORT Approved for public release; distribution is unlimited.
2b. DECLASSIFICATION / DOWNGRADING SCHEDULE	
4. PERFORMING ORGANIZATION REPORT NUMBER(S) CRDEC-CR-88039	5. MONITORING ORGANIZATION REPORT NUMBER(S)
6a. NAME OF PERFORMING ORGANIZATION SRI International	6b OFFICE SYMBOL (If applicable)
6c. ADDRESS (City, State, and ZIP Code) Menlo Park, CA 94025	7a. NAME OF MONITORING ORGANIZATION 7b. ADDRESS (City, State, and ZIP Code)
8a. NAME OF FUNDING / SPONSORING ORGANIZATION CRDEC	8b. OFFICE SYMBOL (If applicable) SMCCR-DDT
8c. ADDRESS (City, State, and ZIP Code) Aberdeen Proving Ground, MD 21010-5423	9. PROCUREMENT INSTRUMENT IDENTIFICATION NUMBER DAAK11-82-0158 10 SOURCE OF FUNDING NUMBERS

PROGRAM ELEMENT NO.	PROJECT NO.	TASK NO.	WORK UNIT ACCESSION NO.

11. TITLE (Include Security Classification)
Infrared Differential Absorption Lidar for Vapor Detection

12. PERSONAL AUTHOR(S)
Carrico, J. P., Phelps, K. R., van der Laan, J., Uthe, E. E., (continued on reverse)

13a. TYPE OF REPORT	13b. TIME COVERED	14. DATE OF REPORT (Year, Month, Day)	15. PAGE COUNT
Contractor	FROM 83 TO 84	1988 February	35

16. SUPPLEMENTARY NOTATION
COR: K. Phelps, SMCCR-DDT, (301) 671-3484

17. COSATI CODES			18. SUBJECT TERMS (Continue on reverse if necessary and identify by block number)
FIELD	GROUP	SUB-GROUP	Standoff detection, DIAL/DISC
17	05	01	Remote detection, Lidar
15	06	03	

19. ABSTRACT (Continue on reverse if necessary and identify by block number)
Ground-mobile and airborne carbon dioxide (CO_2) laser systems were developed to measure vapor clouds using differential absorption lidar (DIAL) techniques. Field testing with the ground-mobile lidar detected a vapor cloud at 7 km using the return signal from a topographic target at a range of 8.5 km. Range-resolved detection enabled mapping of vapor cloud concentration to a range of at least 1 km. The airborne lidar mapped vertically integrated, cross-cloud gas concentrations at 3 km and detected vapor clouds 7 km downwind from the vapor source.
(Keywords)

20. DISTRIBUTION / AVAILABILITY OF ABSTRACT	21. ABSTRACT SECURITY CLASSIFICATION
☒ UNCLASSIFIED/UNLIMITED ☐ SAME AS RPT. ☐ DTIC USERS	UNCLASSIFIED

22a. NAME OF RESPONSIBLE INDIVIDUAL	22b. TELEPHONE (Include Area Code)	22c. OFFICE SYMBOL
SANDRA J. JOHNSON	(301) 671-2914	SMCCR-SPS-T

DD FORM 1473, 84 MAR 83 APR edition may be used until exhausted. All other editions are obsolete.

SECURITY CLASSIFICATION OF THIS PAGE
UNCLASSIFIED

12. Personal Authors (continued)

Holland, P. L., Kawley, J. G., Fletcher, L. D., Warren, R. E., Nielsen, N., Rosengreen, A., and Murray, E. R.

PREFACE

The work described in this report was authorized under Contract No. DAAK11-82-0158. This work was started in 1983 and completed in 1984.

The use of trade names or manufacturers' names in this report does not constitute an official endorsement of any commercial products. This report may not be cited for purposes of advertisement.

This report has been approved for release to the public.

Blank

CONTENTS

Blank

INFRARED DIFFERENTIAL ABSORPTION LIDAR FOR VAPOR DETECTION

I INTRODUCTION

Lidar, in general, and differential absorption lidar (DIAL), in particular, have been developed and used for investigative or diagnostic applications concerned with measurements of natural and industrially induced phenomena. Our general purpose in the work reported here was to apply this technology to the problem of measuring vapor and aerosol phenomena in military environments. More specifically, we sought to demonstrate the feasibility of detecting and mapping battlefield induced aerosols and vapors using active remote sensing systems on ground and airborne platforms.

Both ground-mobile and airborne infrared DIAL systems were developed using commercially available components. These systems were designed for versatility and ease of modification in order to study vapor and aerosol phenomena in typical battlefield environments. They made use of existing hardware components and can be updated to state-of-the-art systems during future development programs. A wide range of field experiments were conducted with these systems.

The designs of the ground-mobile and airborne systems are discussed, their testing and experimental results described, and conclusions presented in this paper.

II DESIGN OF THE DIAL SYSTEMS

The purpose of this work was to develop lidar systems to investigate physical transport phenomena of vapors and aerosols that might occur in battlefields of the future, demonstrate concept feasibility, and establish capabilities and limits of system performance. To expedite achieving these goals, commercially available, off-the-shelf equipment was obtained and assembled. This approach permitted testing early in the program and provided the appropriate experimental flexibility to address scientific and technological issues. Consideration of a state-of-the-art, optimized system for field applications will follow naturally in subsequent developments.

A. Ground-Mobile Breadboard (GMB)

The GMB (Figure 1) was designed for both column-content and range-resolved detection. It possesses real-time display capabilities for field diagnostic purposes, as well as the ability to record all data on magnetic tape for subsequent detailed analyses in the laboratory. The system design consists of a laser transmitter, optical receiver, and control, signal processing, and diagnostic equipment.

1. Laser Transmitter

The transmitter consists of two manually tuned CO_2 TEA lasers configured as shown in Figure 2. The two beams are combined and transmitted coaxially with a variable temporal delay spacing of 10 μs to 10 ms.

A small fraction of each laser beam is diverted for diagnostic measurements of the transmitted peak power, wavelength, and beam alignment. Peak power and pulse shapes are monitored on a pulse-to-pulse basis using the integrating spheres and room-temperature HgCdTe

SOURCE U S Army

TMS-2577

Figure 1. Ground-Mobile Breadboard Lidar System

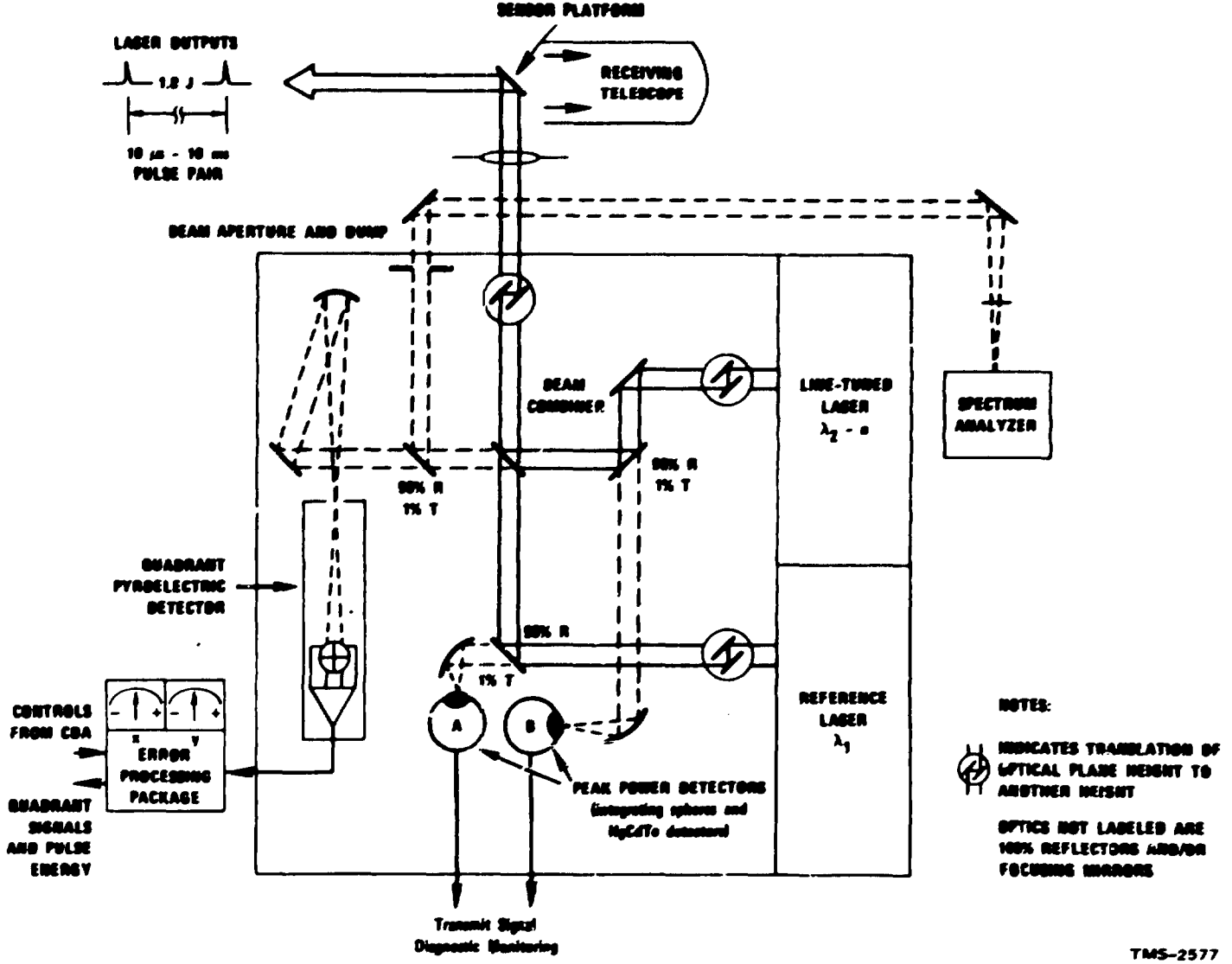

Figure 2. GMB Transmitter

detectors. The laser wavelength is monitored with a spectrum analyzer. Beam position is detected by means of a quadrant pyroelectric detector; results of subtracting the signals from opposing quadrants are displayed on two analog meters to yield beam position error. The quadrant signals are also summed and used to normalize the error signals. The sum signals are recorded as energy monitor signals. The specifications of the transmitter are summarized in Table 1. The lasers operate in a sealed-off configuration with a lifetime of $>10^7$ shots without degradation. The lasers are triggered using a thyratron and exhibit jitter of less than 2.5 ns.

Table 1

GMB LIDAR HARDWARE SPECIFICATIONS

Parameter	Specification
Transmitter Module	
Wavelengths (μm)	9.2-10.8
Energy/pulse (J on 10P20)	3.0
Pulse rate (Hz)	20
Beam divergence (mrad)	6.5H, 3.5V
Mode	Multimode
Pulsewidth (ns gain switch)	90
Beam area (mm x mm)	18 x 36
Receiver Module	
Diameter (in.)	16
Detector	HgCdTe Quadrant
Detectivity (cm $Hz^{\frac{1}{2}}/W$)	4×10^{10}
FOV (mrad)	8
Bandwidth (Hz-MHz)	10-7
Data Module	
Digitization (MHz-bit)	10-12 lin/10-10 log
Energy monitor	Pyroelectric
Wavelength monitor	CO_2 spectrum analyzer
Processor	DEC LSI 11/23
Recording	9-track, 2400 ft
Display	TV of computed data
Visual scene	Color video

2. Optical Receiver

The receiver consists of a f/2.5, 40.6-cm diameter Newtonian telescope with a liquid N_2 HgCdTe quadrant detector (Figure 3). The detectivity of each 1x1-mm detector element is 4×10^{10} cm $Hz^{\frac{1}{2}}/W$. To expand the field of view (FOV) of the receiver, a germanium immersion lens was used to yield an FOV of 8 mrad. Both log and linear output were available for the quadrant sum signal. Beam alignment was monitored on the received signal in a similar fashion to that described for the transmitted signal. The detector and amplifier were mounted in an EMI-shielded box and powered using a 12-V battery.

3. Control, Signal Processing, and Diagnostic Equipment

The lidar control, signal processing and diagnostic subsystems were designed to provide real-time displays of raw signals and processed data, e.g., vapor concentration, and to store all raw data on tape for later analysis. The system used to accomplish this is shown in Figure 4. Trigger pulses that signal laser firings are input to the programmable clock, which in turn triggers the digitizers. Digitized data are transmitted to the microprocessor for averaging and processing to determine concentration and other parameters, and are subsequently displayed on the TV monitor. Video camera data are displayed on the second monitor and recorded to provide visual documentation of scenes involved in the tests.

B. Airborne System

The airborne system (Figure 5) was designed to operate in the SRI Queen Air twin-engine Beechcraft. The design is a simple downward-looking configuration. The specifications of the lidar are similar to those of the ground-mobile system, with the following differences:

1. The use of available laser components compatible with aircraft weight, size, and power constraints limits the laser pulse repetition frequency to 2 Hz.

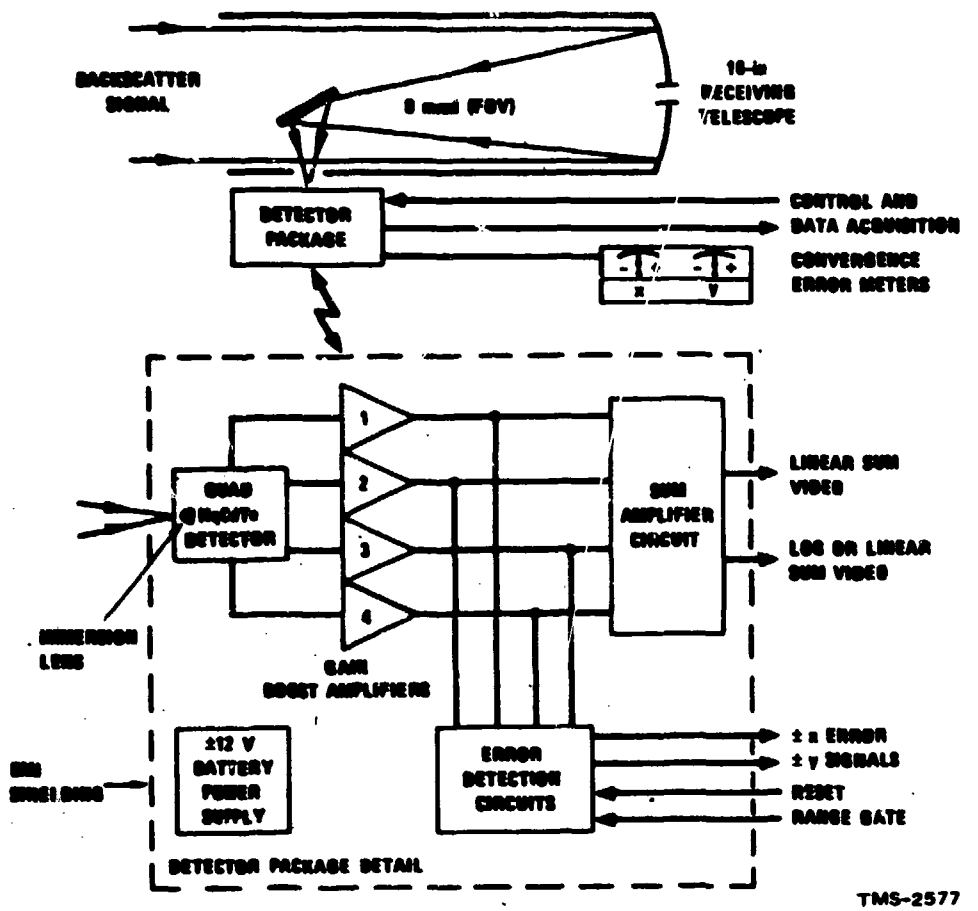

Figure 3. GMB Receiver

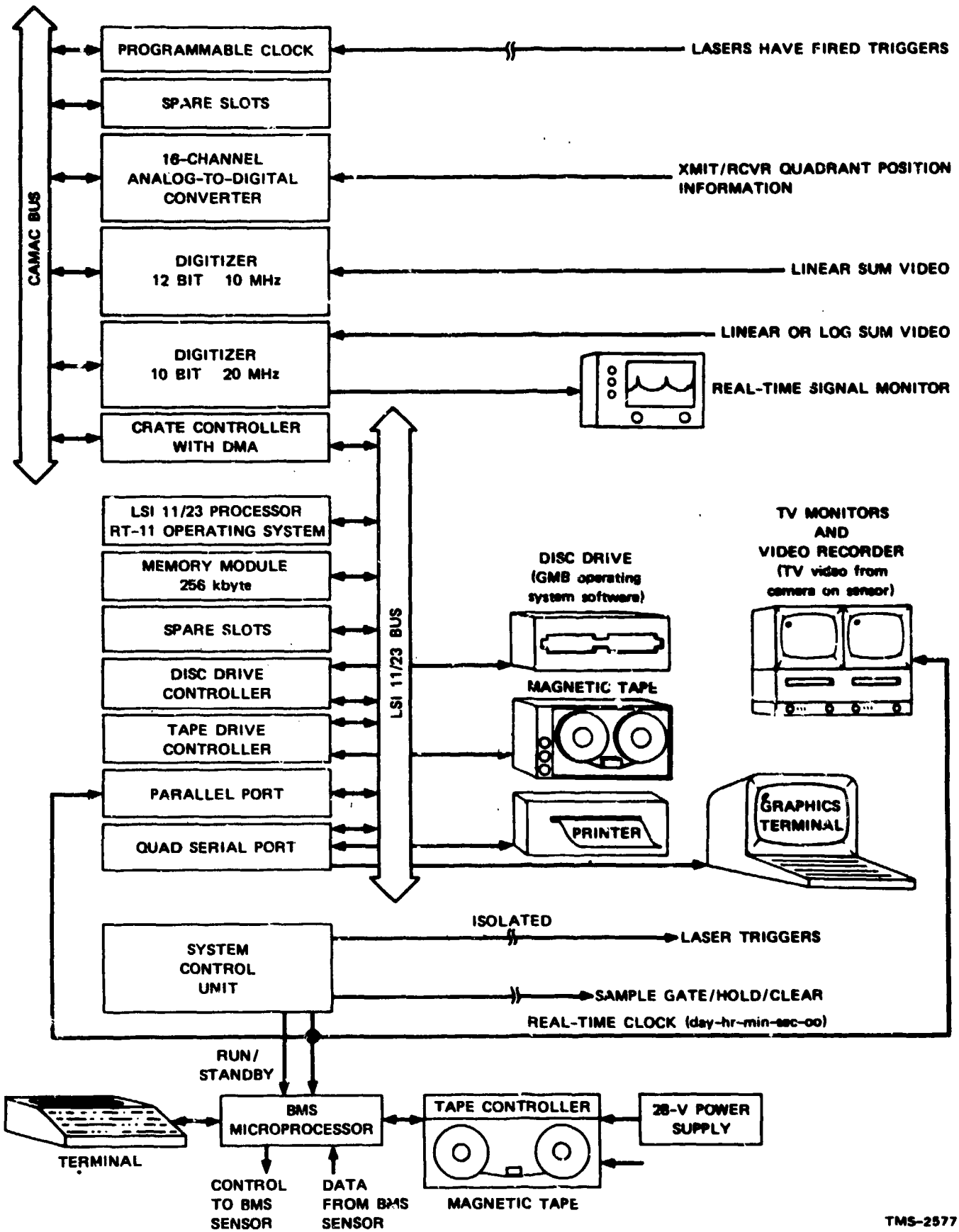

Figure 4. GMB Control and Data Acquisition

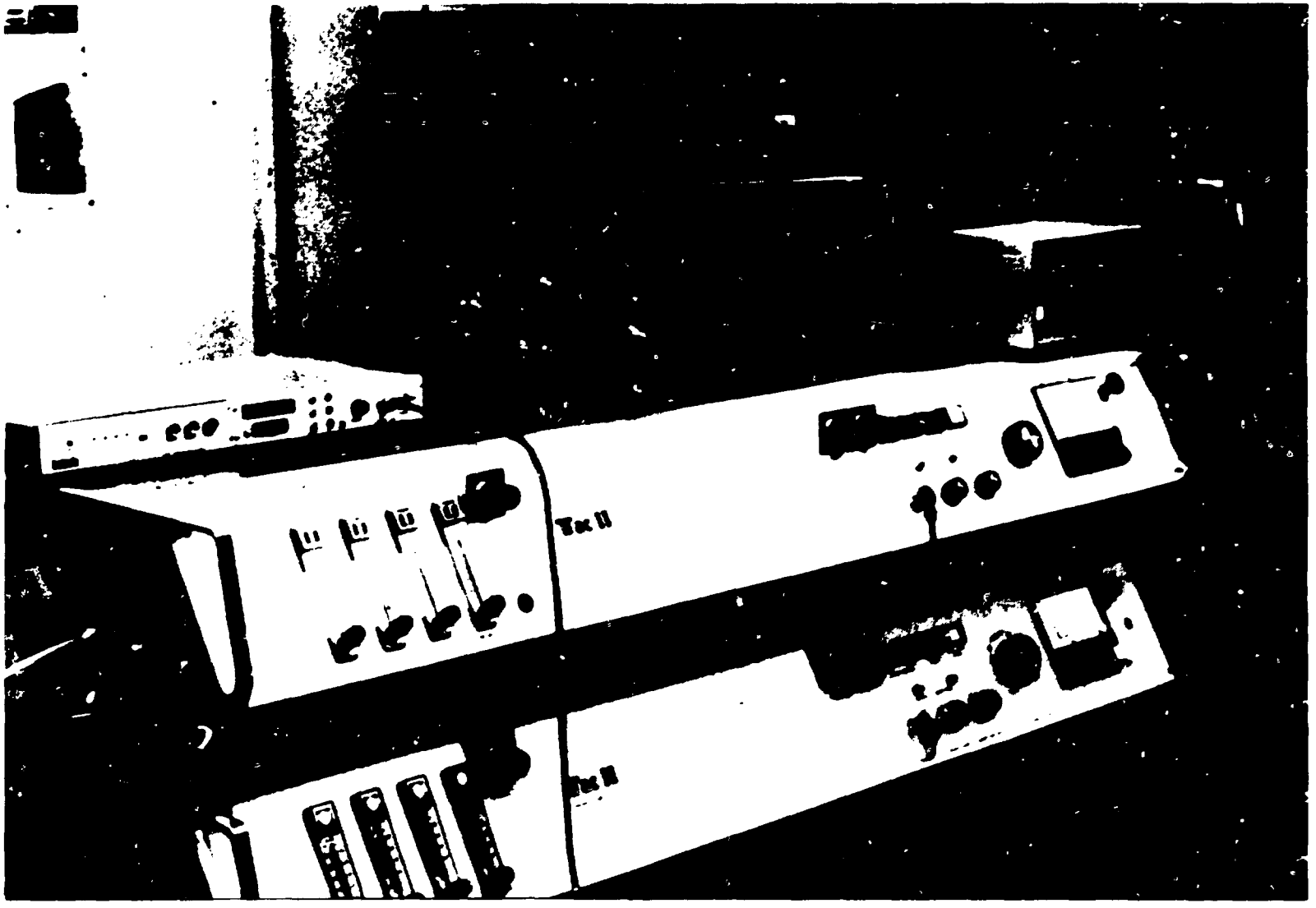

Figure 5. Air-Reconnaissance System

2. The telescope diameter matches the size of the existing port in the aircraft, using a 36-cm Cassegrain configuration.

3. Aircraft payload limitations restrict real-time data processing and display.

4. A linear data channel is used for column-content measurements and a logarithmic channel for range-resolved measurements.

A block diagram of the airborne system is shown in Figure 6. System specifications, based on equipment readily available at the time of the tests, are given in Table 2. The system is expandable to incorporate more recent advances in laser and data analysis equipment that more closely match the performance specifications of the ground-mobile system.

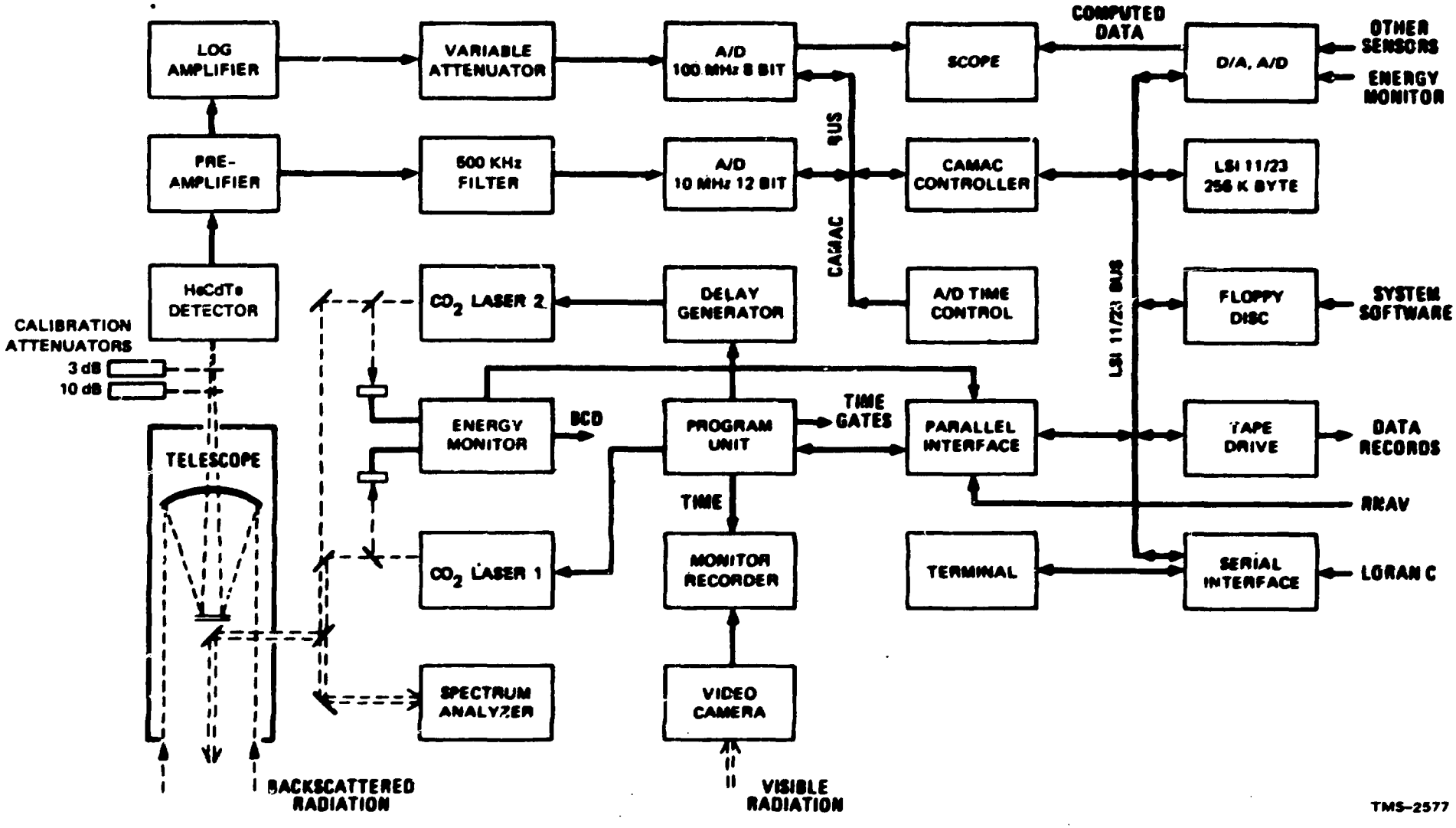

Figure 6. Block Diagram of Airborne System

Table 2

AIRBORNE LIDAR HARDWARE SPECIFICATIONS

Parameter	Specification
Transmitter Module	
Wavelengths (μm)	9.2-10.8 (70 lines)
Energy/pulse (J on 10P20)	1.5 max
Pulse rate (Hz)	2
Beam divergence (mrad)	4.3E, 2.6V
Mode	Multimode
Pulsewidth (ns gain switch)	100
Beam area (mm x mm)	15 x 18
Transmit interval (μs)	30 (adjustable)
Receiver Module	
Diameter (cm)	35 (14 in.)
Detector	HgCdTe
Dectectivity (cm $Hz^{1/2}/W$)	$4x10^{10}$
FOV (mrad)	6
Bandwidth (Hz-MHz)	10-7
Data Module	
Digitization (MHz-bit)	10-12 lin/100-8 log
Energy monitor	Pyroelectric
Wavelength monitor	CO_2 spectrum analyzer
Processor	DEC LSI 11/23
Recording	9-track, 600 ft, 1600 bpi
Display	A-scope (lin or log)
Visual scene	Color video

III FIELD EXPERIMENTS AND RESULTS

A. Experimental Conditions

Experiments were initiated in the summer of 1984 at the U. S. Army Dugway Proving Ground (DPG), Utah, approximately 100 miles southwest of Salt Lake City.

The site is a high desert with flat terrain partially covered with low brush. Daytime temperatures were typically 90-95°F. Column-content experiments were conducted using Granite Mountain, located 8.5 km away, as the topographic reflector. Range-resolved measurements were performed at shorter ranges within or near the test site.

The vapor used was dimethyl methylphosphonate (DMMP), which is a liquid at room temperature but vaporizes readily when aerosolized or spread on surfaces.

The DMMP vapor was disseminated using truck-mounted sprayers (Figure 7). One to three trucks were used, depending on the experiment. Each truck used pressurized nitrogen bottles to aerosolize liquid DMMP from a 2-m long spray bar about 3 m above ground. The aerosol quickly evaporated, forming a vapor cloud downwind. Each truck had a 20-gallon capacity and a capability of disseminating its load in 20 min.

SOURCE: U.S. Army

TMS-2577

Figure 7. DMMP Disseminator

The degree of interference from various smokes such as hexachloroethane (HC), white phosphorous (WP), and red phosphorous (RP) was also investigated. A smoke release from a generator located immediately in back of the truck is also shown in Figure 7. Smokes were also used to assist the aircraft pilot in locating otherwise invisible vapor clouds.

B. Lidar Return Signals

Typical return signals from the atmosphere and a topographic target are shown in Figure 8. The left-hand column has a full scale of 3 km and shows the detail of the return signal from naturally occurring aerosols which yield range-resolved data. The right-hand column has a full scale of 9 km and shows the topographic return signal from Granite Mountain which yields column-centered data. Each scope display shows the return signals for two wavelengths--one not absorbed, λ_A, and one absorbed, λ_B, by DMMP vapor. DMMP was released upwind of the GMB and drifted through its line of sight at a range of 1 km. The top two displays show the signals before DMMP reached the line of sight; note that both the absorbed and nonabsorbed signals are nearly parallel, indicating no differential absorption and hence no presence of DMMP. The middle two displays show the effect of DMMP on both the aerosol and topographic target return signals for λ_B. The bottom two displays show the effect of a very large concentration of DMMP, which decreases the return signal for λ_B below the noise at a range of less than 1.5 km and totally attenuates the topographic return signal.

These types of data, digitized and processed in real time and again in more detail in the laboratory, are described in more detail below.

C. Column-Content Test

Detection of a cloud of DMMP 7 km away from the lidar system was attempted using topographic reflection from Granite Mountain at a range of 8.5 km. The received raw energy data for the topographic return were plotted versus elapsed time (Figure 9). The signal from the non-absorbed wavelength (laser A) is fairly constant, with the only variations due to overall system noise. The signal from the absorbed

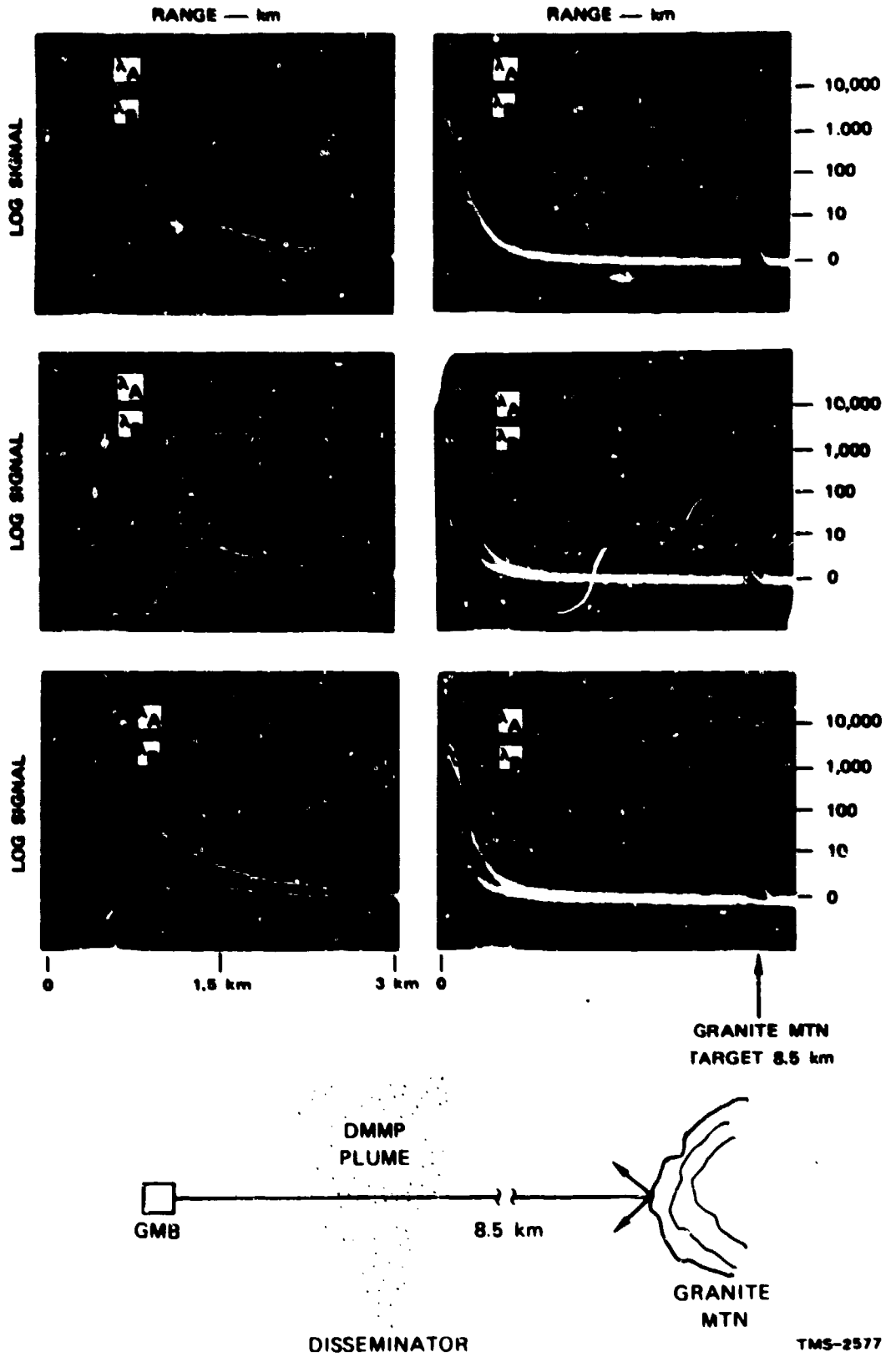

Figure 8. Typical Lidar Signals Showing Absorbed and Nonabsorbed Wavelengths. The top pair shows the signals with no DMMP present. The middle pair were taken with some DMMP. The bottom pair with a large amount of DMMP.

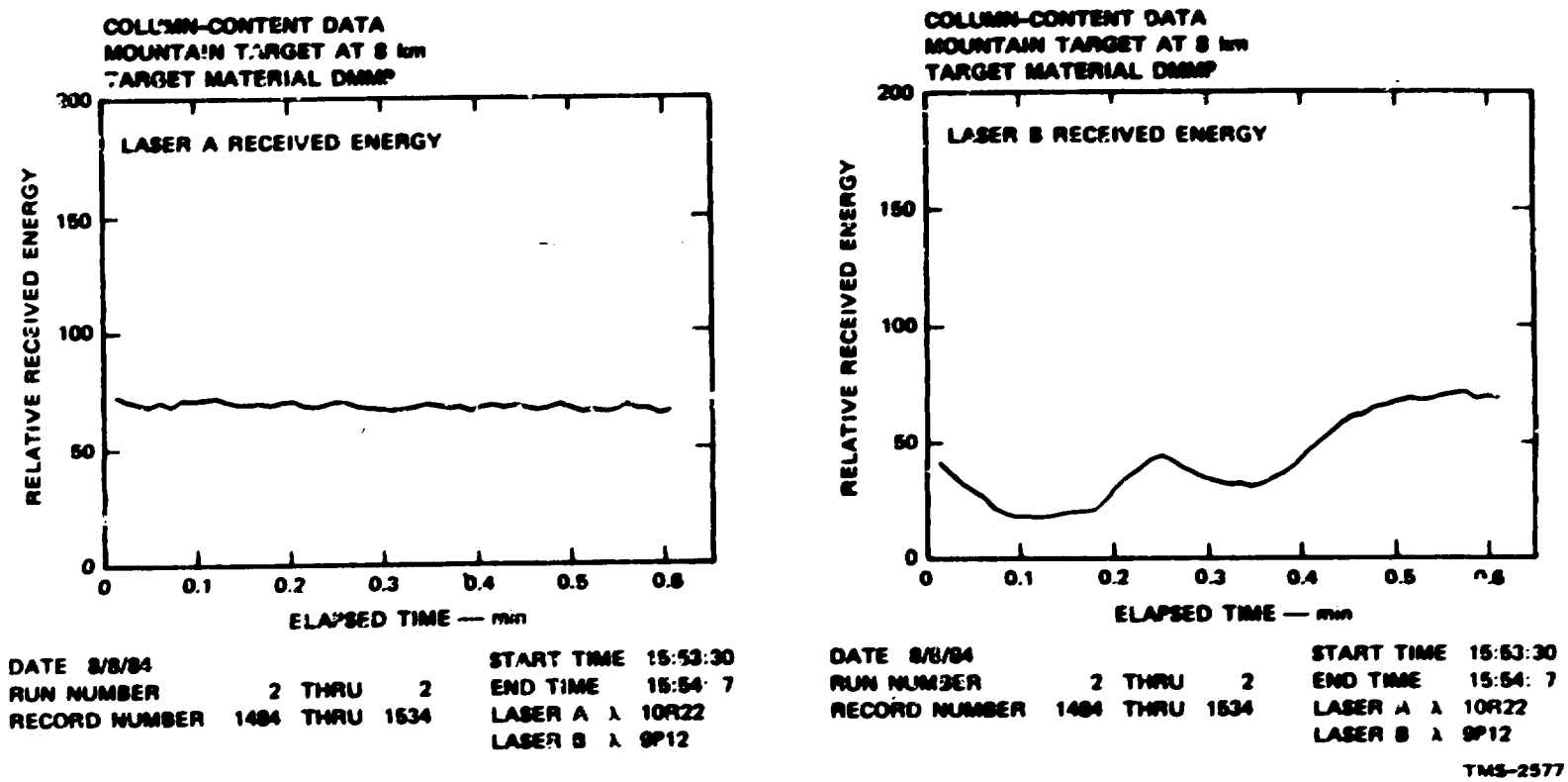

Figure 9. Raw Data From Column Content Tests

wavelength (laser B) shows two substantial local minima that are caused by absorption by clouds of DMMP. When processed using Beer's law, these data yield the concentration-times-path-length products (CL) shown in Figure 10. The two clouds of DMMP are shown to have peak CLs of 400 and 200 mg/m^2. Following the passage of the second cloud, the CL product decreases to near zero, and subsequently its variation reflects the propagation of system noise into the CL product calculations. The standard deviation of the CL data obtained with no absorbing vapor is one measure of the sensitivity of the system. For these data the standard deviation was computed to be 9 mg/m^2.

D. Range-Resolved Test

Range-resolved tests were conducted with DMMP released with HC smoke. The line of sight of the lidar was held stationary to observe the concentration pattern of the cloud drifting through the FOV.

The real-time display of raw data in the range-resolved mode is shown in Figure 11. The top plots show the log of the range-corrected signal versus range. The plot on the left is nonabsorbed data (λ_A); all displayed return signals lie nearly on top of each other. The top right-hand plot is the absorbed return signal (λ_B), which shows a sequence of decreasing signal returns caused by an increasing concentration of DMMP. The lower left plot shows the integrated concentration (CL) of the cloud with monotonically increasing values of CL up to approximately 650 mg/m^2. The right lower plot shows concentration versus range with peak values of 1.5 mg/m^3. Beyond approximately 800 m, the raw data exhibit mostly noise because of signal loss due to substantial absorption by the cloud and $\frac{1}{r^2}$ effects associated with increasing range.

These data were processed and prepared in a 3-D format (Figure 12). The first minute of data is background with neither DMMP nor smoke present. The occasional spikes, noticeable especially at longer ranges, are caused by random noise of the system that has become larger locally than the threshold value of 0.25 mg/m^3, which was chosen to establish the threshold plane. HC smoke then drifted through the line of sight,

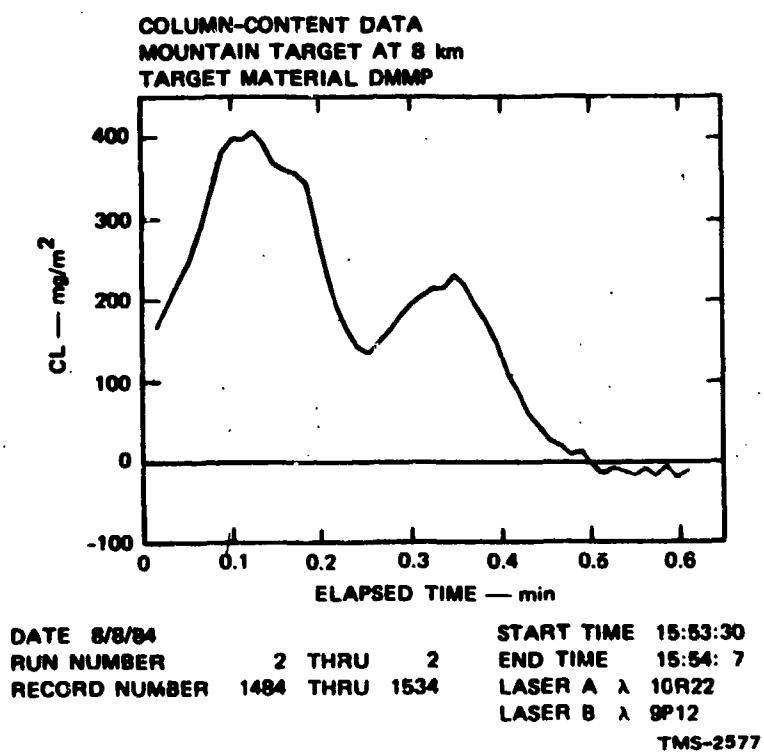

Figure 10. Column-Content Detection Data

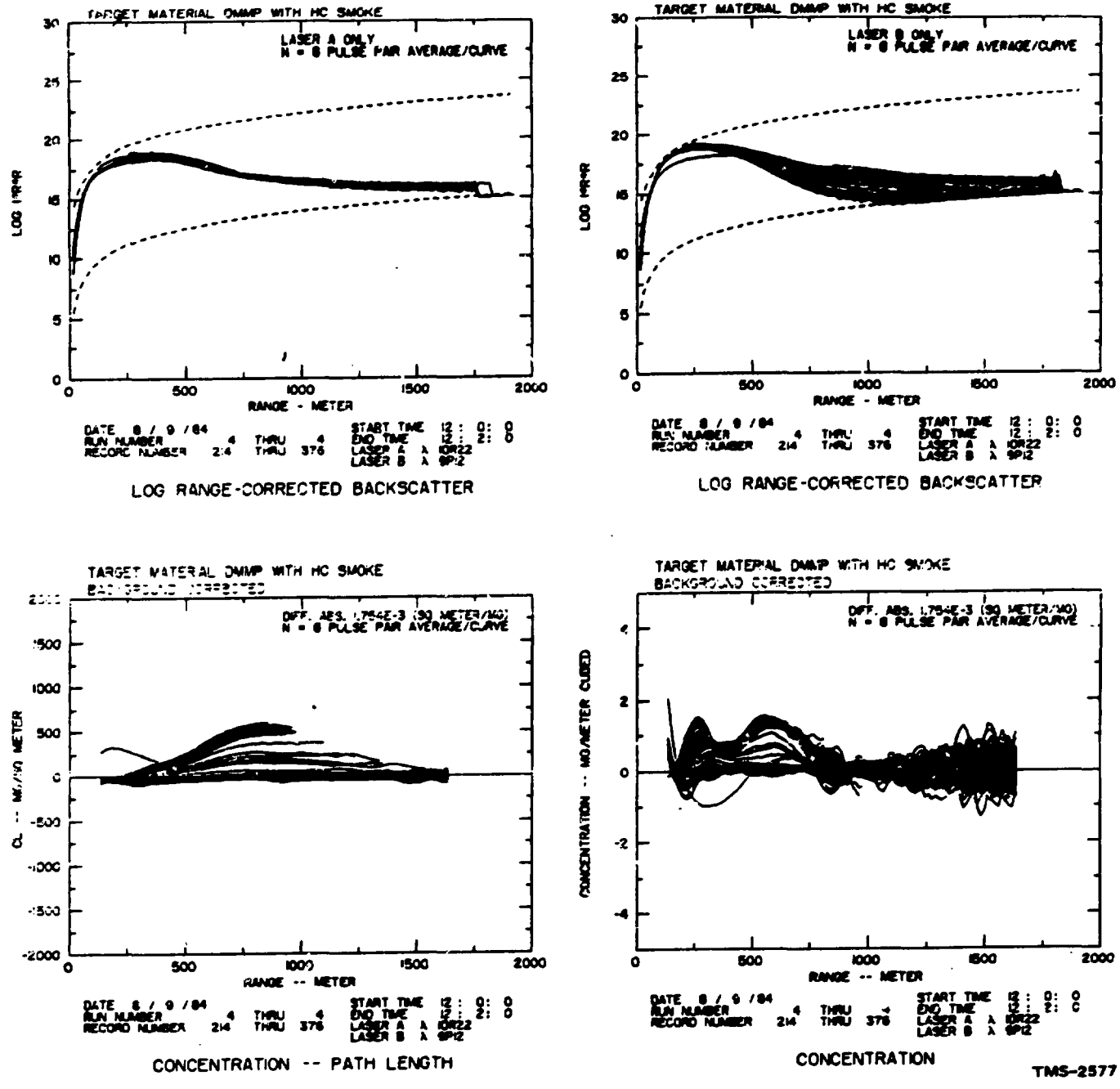

Figure 11. Real-Time Display of Range Resolved Data in DMMP Test

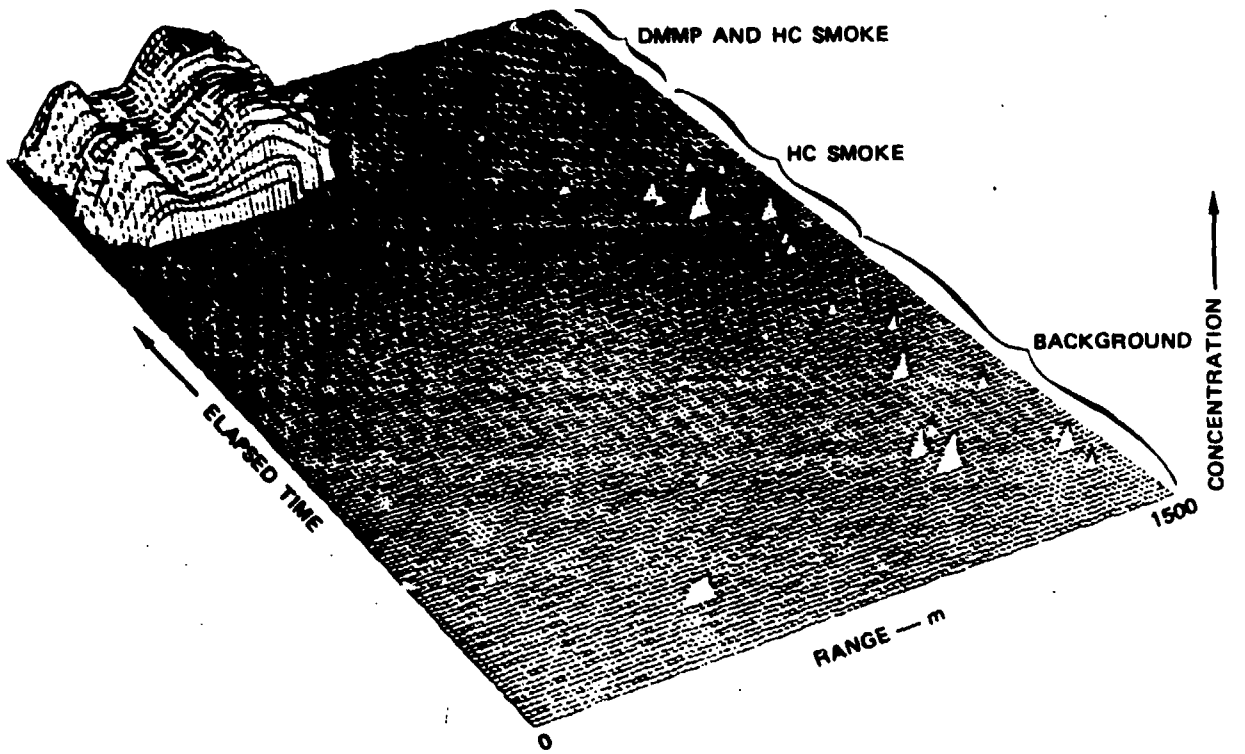

DATE 8/9/84
RUN NUMBER 4 THRU 4
RECORD NUMBER 214 THRU 376

START TIME 12: 0: 0
END TIME 12: 2: 0
LASER A λ 10R22
LASER B λ 9P12

TMS-2577

Figure 12. Measured Cloud of DMMP with HC Smoke in 3-D Format

causing no apparent change in the random and/or systematic error of the system. Next, DMMP was released simultaneously with HC smoke and the bifurcated cloud shown in the plot rose well above the threshold plane. The peak concentration detected was 1.5 mg/m^3, and the standard deviation of the background data at 1 km was calculated to be 0.09 mg/m^3 when averaging 8 pulse pairs of data (0.4 s of data).

E. Dual Cloud Test

Two clouds, each from a different location and type of source, were generated and detected. The clouds were disseminated as shown in Figure 13. The cloud closest to the GMB was generated by spraying the ground with DMMP, which evaporated over a period of 20 minutes. The cloud farthest from the GMB was generated by directly spraying DMMP into the air. Typical vapor cloud detection results are displayed in Figure 14. The first cloud encountered was somewhat smaller in concentration because it is the result of secondary evaporation. Note that, as time passes, the concentration of the cloud decreases and then increases. These changes indicate the influence of the micrometeorological conditions. For example, clouds may drift out of the line of sight, causing voids in detected concentrations, or, as indicated midway during the measurement period, clouds may separate completely and exhibit much smaller concentrations. At the end of the elapsed time, the clouds remerged with a significant increase in concentration.

F. Test of Vertical Scanning

The ability to detect and map clouds vertically was demonstrated with vertical scanning of the system. Typical resulting data are shown in Figure 15. In this display, the cloud is plotted as a solid line when the concentration exceeds a threshold concentration of 0.25 mg/m^3. The detected cloud was found to have a maximum height of 20 m and to occur between 600 m and 1000 m in range.

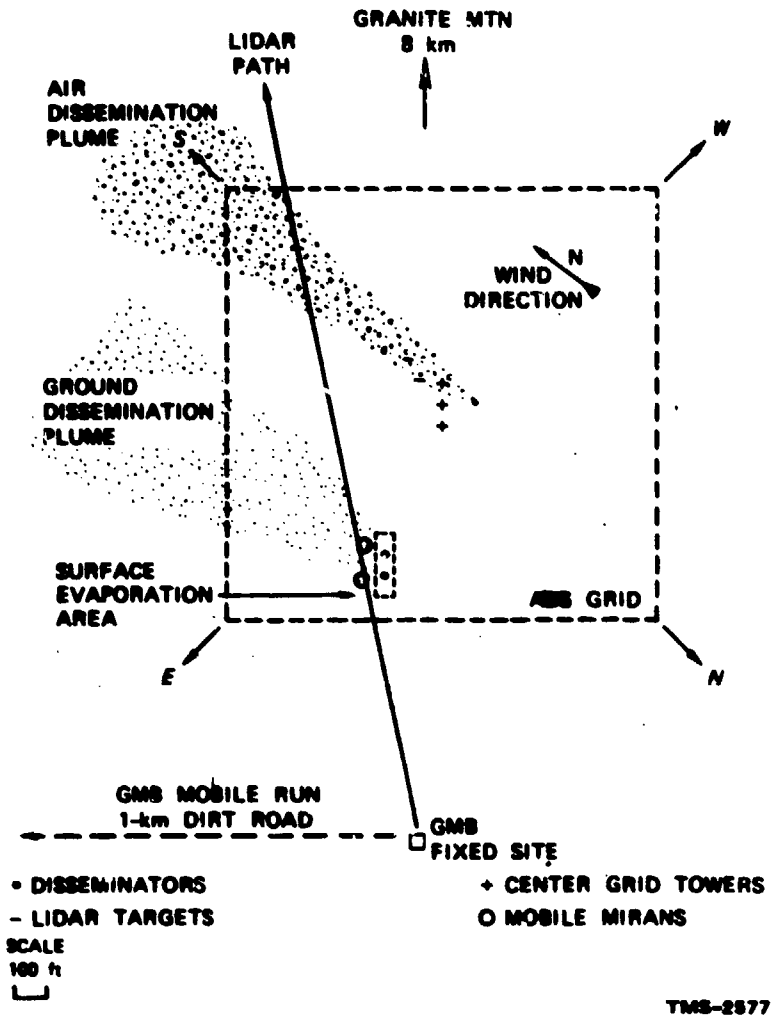

Figure 13. Dual Plume Test Configuration

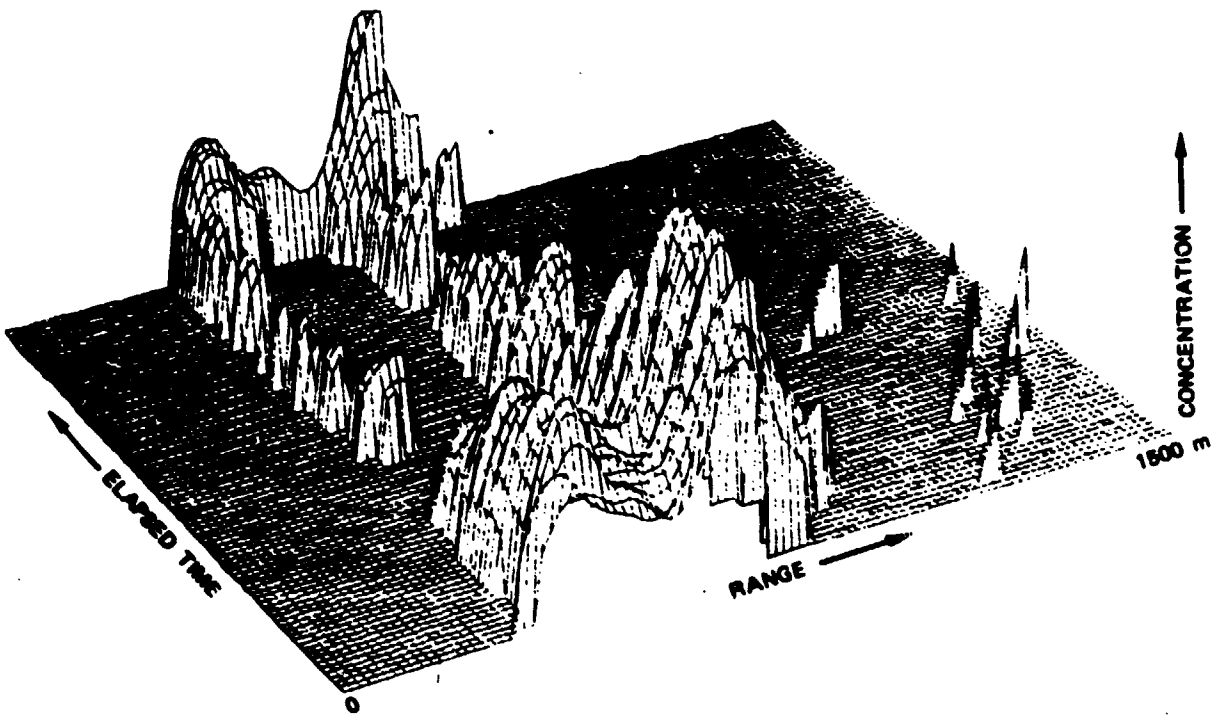

DATE 7/10/84
RUN NUMBER 2 THRU 2
RECORD NUMBER 187 THRU 270

START TIME 10:26: 1
END TIME 10:26: 3
LASER A λ 10R22
LASER B λ 9P16

TMS-2577

Figure 14. Dual Plume Test Results

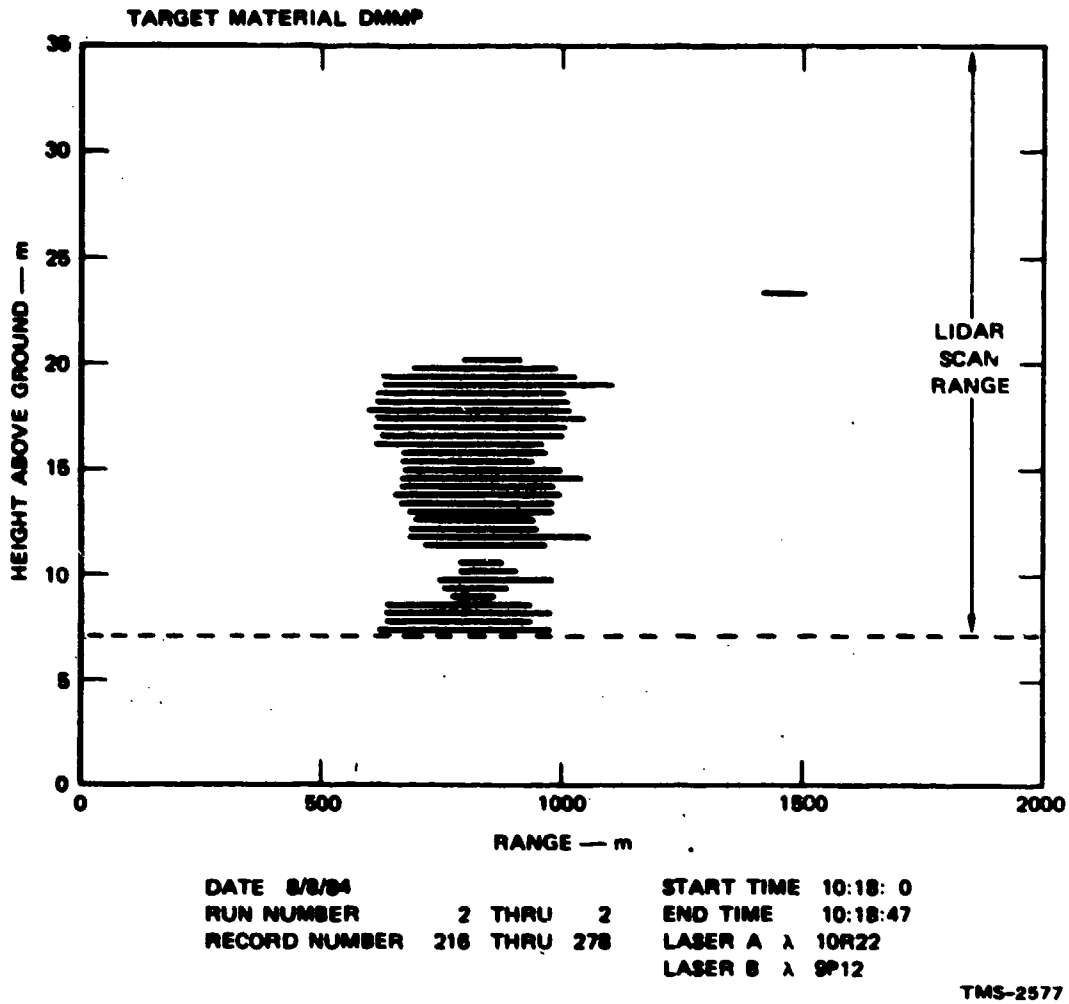

Figure 15. Resulting Data From Vertical Scanning

C. Airborne Detection Using Topographic Scattering

Measurements with airborne lidar were taken along the oval flight pattern shown in Figure 16. The aircraft repeatedly crossed the plume at locations close to the source (which would tend to have larger concentrations and narrower clouds) and far from the source (which would tend to have smaller concentrations and wider clouds). An example of the resulting column-content data is presented in Figure 17. The diamonds represent turnaround points for the aircraft; thus, one would expect to see a cloud between each pair of diamonds. As shown by the data, the clouds tend to be wider at larger downwind distances. The airborne lidar detected vapor clouds 7 km downwind of their source and might have detected clouds farther downwind except for flight restrictions imposed by other operations in the area.

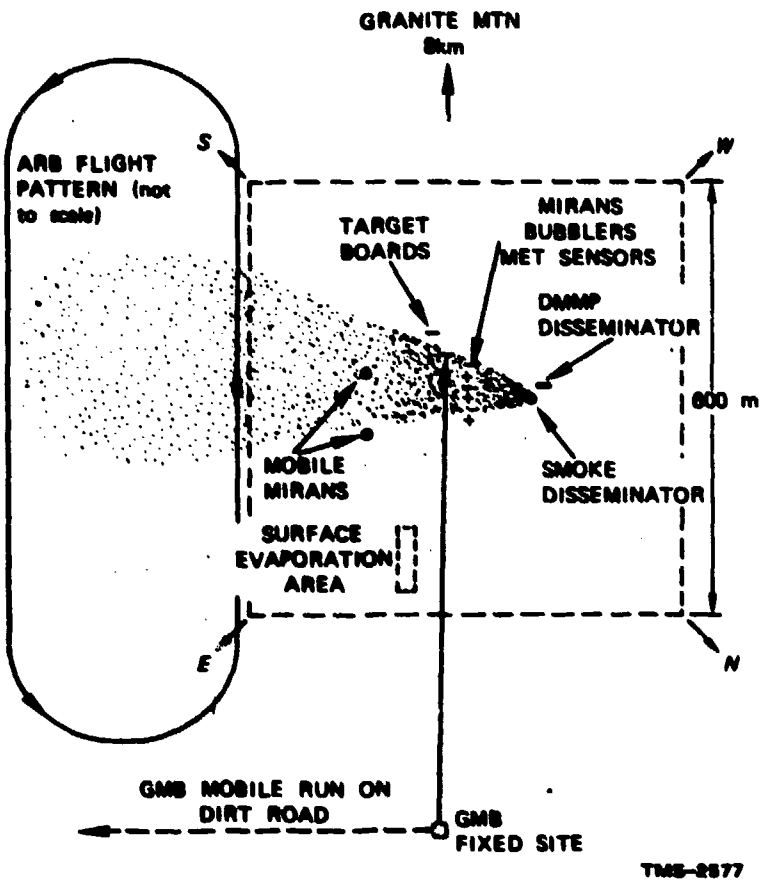

Figure 16. Aircraft Flight Path and Vapor Disseminator

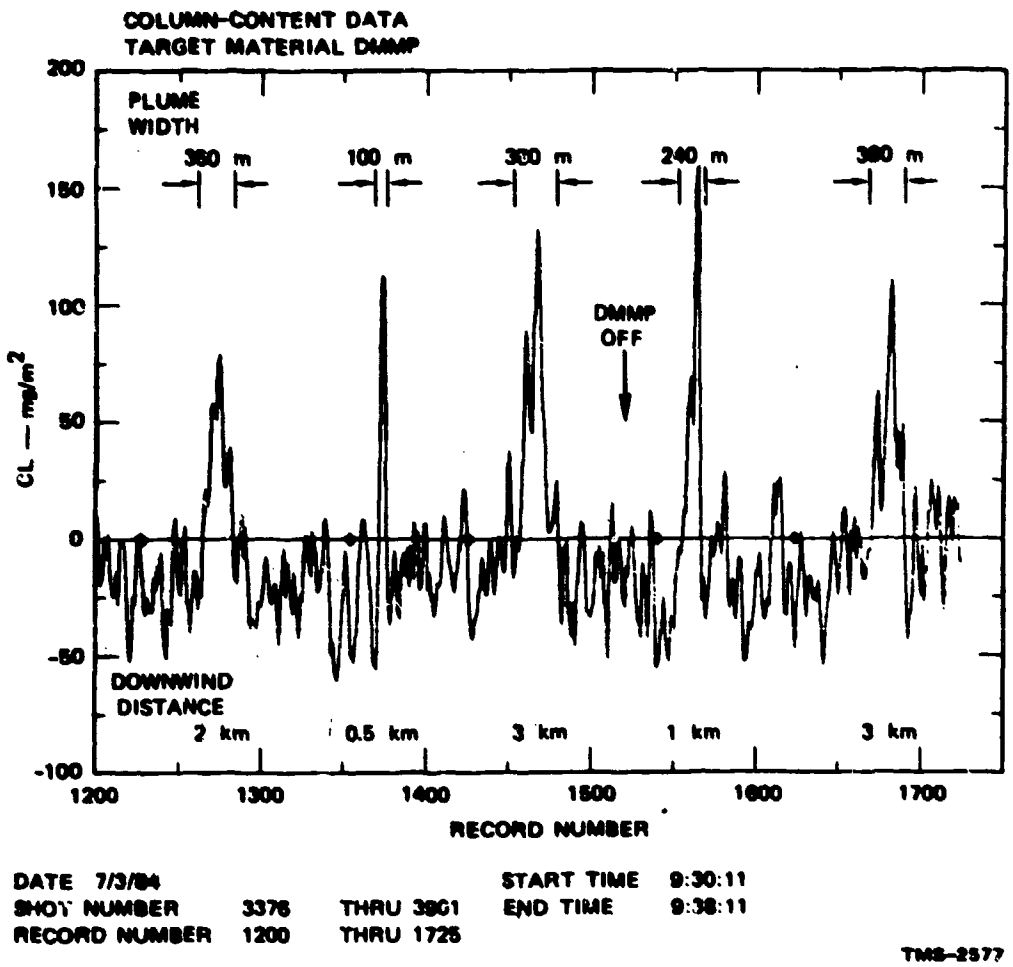

Figure 17. Airborne Lidar Results in Column-Content Operation

IV CONCLUSIONS

Ground-mobile and airborne CO_2 lidar systems were developed to measure vapor and aerosol clouds. The lidars were operated in the field using DMMP as the target vapor to examine their performance capabilities. Column-content detection of a DMMP cloud 7 km away using topographic reflection from 8.5 km away yielded a measured uncertainty of 9 mg/m^2. Range-resolved tests were used to map DMMP cloud concentrations, and the measured uncertainty at 1 km in range was 0.09 mg/m^3. Two clouds were generated, detected, and distinguished from one another to demonstrate detection of a cloud through a cloud. Also, measurements of vapor evolving from liquid on a surface were demonstrated.

The airborne lidar detected vapor clouds up to 7 km downwind of their source and was limited from detection farther downwind by aircraft flight restrictions, not the sensitivity of the system.

Work is underway to upgrade the detection and data processing capabilities of these systems. These improvements will then be followed by further testing at DPG. Also, an effort is underway to address equipment miniaturization issues associated with fielding practical lidar systems for military applications.